SCIENCE CHINA
Technological Sciences

February 2012 Vol.55 No.2: 421–436
doi: 10.1007/s11431-011-4682-8

Giant piezoresponse and promising application of environmental friendly small-ion-doped ZnO

PAN Feng*, LUO JingTing*, YANG YuChao, WANG XuBo & ZENG Fei

Key Laboratory of Advanced Materials, Department of Materials Science and Engineering, Tsinghua University, Beijing 100084, China

Received September 14, 2011; accepted October 25, 2011; published online December 28, 2011

In recent years, with the growing concerns on environmental protection and human health, new materials, such as lead-free piezoelectric materials, have received increasing attention. So far, three types of lead-free piezoelectric systems have been widely researched, i.e., perovskites, bismuth layer-structured ferroelectrics, and tungsten-bronze type ferroelectrics. This article presents a new type of environmental friendly piezoelectric material with simple structure, the transition-metal(TM)-doped ZnO. Through substituting Zn^{2+} site with small size ion, we obtained a series of TM-doped ZnO with giant piezoresponse, such as $Zn_{0.975}V_{0.025}O$ of 170 pC/N, $Zn_{0.94}Cr_{0.06}O$ of 120 pC/N, $Zn_{0.913}Mn_{0.087}O$ of 86 pC/N and $Zn_{0.988}Fe_{0.012}O$ of 127 pC/N. The tremendous piezoresponses are ascribed to the introduction of switchable spontaneous polarization and high permittivity in TM-doped ZnO. The microscopic origin of giant piezoresponse is also discussed. Substitution of TM ion with small ionic size for Zn^{2+} results in the easier rotation of noncollinear TM-O1 bonds along the *c* axis under the applied field, which produces large piezoelectric displacement and corresponding piezoresponse enhancement. Furthermore, it proposes a general rule to guide the design of new wurtzite semiconductors with enhanced piezoresponses. That is, TM-dopant with ionic size smaller than Zn^{2+} substitutes for Zn^{2+} site will increase the piezoresponse of ZnO significantly. Finally, we discuss the improved performances of some TM-doped ZnO based piezoelectric devices.

ZnO, lead-free piezoelectric, doping modification, piezoresponse enhancement

Citation: Pan F, Luo J T, Yang Y C, et al. Giant piezoresponse and promising application of environmental friendly small-ion-doped ZnO. Sci China Tech Sci, 2012, 55: 421–436, doi: 10.1007/s11431-011-4682-8

1 Introduction

Piezoelectric materials are key materials for the fabrication of various transducers, pressure sensors and actuators, piezoelectric oscillator and actuators, transformer, surface acoustic wave (SAW) and bulk acoustic wave (BAW) devices, which are widely used in the fields of information, energy, machinery, electronics and national defense [1–4]. Because of their excellent piezoelectric property, lead (Pb) based piezoelectric materials, such as lead zirconate titanate (PZT), is one of the most widely exploited and extensively used piezoelectric materials [5, 6]. However, Pb-based piezoelectric materials have a critical disadvantage for their Pb content is higher than 60% by weight. Pb is highly toxic and its toxicity can be further enhanced due to its easy volatilization during processing [7, 8]. Besides, its disposal is also potentially environmentally toxic. Thus, the use and processing of Pb-based piezoelectric materials may contaminate the environment and damage human health, which limit their applications. With the raise of environmental consciousness, lead-free piezoelectric materials have received increasing attention and it is a prevailing trend that environmental friendly lead-free piezoelectric materials will replace Pb-based piezoelectric materials [9, 10]. Currently, three types of lead-free piezoelectric materials are being

*Corresponding author (email: panf@mail.tsinghua.edu.cn, luojt07@hotmail.com)

considered as potential alternatives to Pb-based piezoelectric materials for specific applications. They are perovskite systems (bismuth sodium titanate [11], alkali niobates [12], etc.), non-perovskites such as bismuth layer-structured ferroelectrics (BLSF), and tungsten-bronze type ferroelectrics [13, 14]. However, they cannot match the overall performance of Pb-based piezoelectric materials, and moreover, the compositions and the structures of these materials are complex, which may decrease the stability of their property and increase the difficulty in application.

Zinc oxide (ZnO) possesses non-centro-symmetric crystal structure and exhibits piezoelectricity. As a piezoelectric material, ZnO has various advantages. Firstly, it has the strongest piezoelectric response among the tetrahedrally bonded semiconductors [15]. Secondly, it is structurally simple and easy to fabricate and magnetron sputtering which is widely used in industry for mass production can fabricate high quality ZnO films. Besides, ZnO film is compatible with the semiconductor process. Therefore, ZnO has been widely used as sensors and actuators in microelectromechanical systems and as SAW and BAW devices in communication field [16, 17]. However, the performance improvement of piezoelectric device demands stronger piezoelectric behavior and piezoresponse d_{33} as the important parameter for evaluating piezoelectric property of ZnO demands improvement. For ZnO bulk, the piezoresponse is ~9.9 pC/N [18] and for an oriented ZnO film, the piezoresponse is only ~12.4 pC/N [19], which is approximately one or two orders of magnitude lower comparing with Pb-based piezoelectric materials. If the piezoresponse of ZnO could be increased and comparative to that of Pb-based piezoelectric materials, the performances of available ZnO-based piezoelectric devices would be improved significantly. Additionally, the enhanced piezoelectricity could widely extend the application field of ZnO. Since ZnO not only possesses high piezoelectricity, but is environmental friendly and abundant in raw materials, it can be used as a new type of promising environmental friendly lead-free piezoelectric materials to replace Pb-based piezoelectric materials. Therefore, the enhancement of piezoelectric properties of ZnO is of great significance. Many researchers have focused on pure ZnO film and attempted to improve its properties by optimizing the preparation conditions, but the results are not distinct [20–22]. Doping is a good method to improve the piezoelectric properties of Pb-based piezoelectric materials [23–27], and there are many successful examples to improve the properties of ZnO films by doping. Doping with Al and Ga can improve the quality and conductivity of ZnO films [28, 29]. Co-doping can induce the room-temperature ferromagnetism in Co-doped ZnO films [30–35]. Doping with V, Cu and Ag can improve the photoluminescence properties of ZnO films [36–38]. Moreover, one can optimize the properties of ZnO and even obtain the electro-optic, magneto-optic, acousto-electronic and acousto-optic properties of ZnO via doping [39]. In the past few few years, we have tried to modify ZnO films by transition-metal (TM)-doping and successfully improved its piezoresponse. We obtained doped-ZnO with giant piezoresponse, $Zn_{0.975}V_{0.025}O$ of 170pC/N [40], $Zn_{0.94}Cr_{0.06}O$ of 120pC/N [41], $Zn_{0.913}Mn_{0.087}O$ of 86 pC/N and $Zn_{0.988}Fe_{0.012}O$ of 127 pC/N [42, 43]. The macroscopic and microscopic mechanisms were studied by systematical experiments and characterizations. We proposed a general rule describing the impact of doping on the piezoresponse of ZnO films. That is, when the doped ion substitutes for Zn^{2+} site, doping ZnO with a small ion can produce enhanced piezoresponse whereas doping ZnO with a big ion results in a decreased piezoresponse. This rule is useful for guiding the design of new wurtzite semiconductors with enhanced piezoresponses. The modified ZnO films with high piezoresponses can be used as environmental friendly lead-free piezoelectric materials, and the rule provides a new way for seeking environmental friendly lead-free piezoelectric materials, which would be a stimulant for growing research on this subject. This has motivated us to come up with a review article with the hope that it would not only give further inspiration to the researchers who have been already working on ZnO films and devices, but also draw the attention of researchers who work on traditional lead-free piezoelectric materials as well as other researchers. In this article, we comprehensively present the effects of various dopants on the piezoresponse of ZnO films. Recent progress in doped ZnO based piezoelectric devices is also discussed.

2 Experimental procedure

2.1 Film growth of TM-doped ZnO

Doped ZnO films are generally deposited by pulsed laser deposition (PLD) [44–48], magnetron co-sputtering [49–55], including direct current (DC) reactive and radio-frequency (RF), molecular beam epitaxy (MBE) [56–60], chemical vapor deposition [61, 62] and sol–gel methods [63–67]. It is known that piezoelectricity is related to the crystallographic quality of ZnO films and high *c*-axis orientation can lead to good piezoelectricity of ZnO films [68–72]. However, there is no conclusion on which deposition method is the best for fabricating piezoelectric ZnO films. Owing to low-cost, high efficiency, easy control, and the production of uniform films of large size, magnetron sputtering is not only used in labs but also widely used in industry for ZnO films growing.

The choice of substrate for growing ZnO piezoelectric films depends on the characterization and the application of ZnO films after deposition. Due to its low mismatch with the film, Al_2O_3 (001) is suitable for fabricating ZnO piezoelectric films of high crystallinity [73]. Besides, with high SAW phase velocity, it is also suitable for the fabrication of ZnO based thin film SAW devices with high frequency. There are also other substrates for fabricating ZnO based thin film high frequency SAW devices, such as diamond,

diamond-like carbon films, SiC [74–77]. Other substrates suitable for the deposition of TM-doped ZnO films are Si [78, 79], AlN/Si [80, 81], SiO_2/Si [82–84], and $LiNbO_3$ [85].

Generally, piezoelectric devices require ZnO films of high quality and high resistivity. To achieve the requirement, one effective method to fabricate TM-doped ZnO films is to select pure metal targets of Zn and TM with abundant oxygen. The relative sputtering area of TM chips or pieces attached around the sputtering race track of Zn target is adjusted to control the TM composition in TM-doped ZnO films. In general, the doping concentration is no more than 12 at.% for higher concentration may deteriorate the crystal quality of ZnO films, which will decrease the piezoelectric properties. The working gas is a mixture of argon and oxygen at various pressures, which can greatly affect the local structure, the electric properties and piezoelectric properties of ZnO films. It is found that high oxygen partial pressure can result in high resistivity of TM-doped ZnO films, which is suitable for piezoelectric application. The thickness of the samples can be determined by the characterization and the application of ZnO films after deposition. Other experiment conditions should be optimized for fabricating high quality, high resistivity and high piezoelectricity of the films.

2.2 Characterization techniques

To understand the local structure and corresponding piezoelectric behavior of TM-doped ZnO, and to accurately detect the chemical information for doping elements at very low concentration, highly sensitive characterization techniques are critical. After deposition, the accurate content of TM in samples can be characterized by X-ray fluorescence (XRF), energy-dispersive X-ray spectroscopy (EDS) and inductively coupled plasma (ICP) atomic emission spectroscopy. The structure and crystalline quality of the films can be characterized by X-ray diffraction (XRD) in the Bragg-Brentano and rocking curve. The state and site of doping elements can be predicted by comparing the positions of diffraction peaks between doped and undoped ZnO films [86–88]. High-resolution transmission electron microscopy (HRTEM) imaging, selected area diffraction (SAD) and field-emission scanning electron microscopy (FE-SEM) can be used to identify interface bonding, to study structural characteristics, and to observe the surface morphology and whether small nanoclusters are present in the films. X-ray photoelectron spectroscopy (XPS) can be used to determine the valence state of the specific element [89–92].

X-ray absorption spectroscopy (XAS), including TM *K*-edge [93–97], TM *L*-edge and its interpretation are used to elucidate the local structure [98–105]. This technique is recently attracting increasing interest due to its promise of providing local chemical information for complex materials and its sensitivity to subtle differences in local environment, which is helpful for a better understanding of the changes of the local environment and the piezoelectricity. If the state of a trace amount of TM dopant cannot be determined using a single characterization technique, we can use several different methods to investigate the local TM structure.

As mentioned above, an important parameter for evaluating the piezoelectricity of ZnO films is piezoresponse d_{33}, and there are various methods for measuring and calculating its piezoresponse value [106–109]. One of the best methods is to use atomic force microscopy (AFM) to detect small piezoelectric displacements when an electric field is applied on ZnO films, and the piezoresponse magnitude can be calculated based on the converse piezoelectric effect [106]. During the measurements, it can apply a conductive rhodium coated silicon cantilever with a spring constant of 1.9 N/m, a resonant frequency of 28 kHz, and an integrated tip of about 10 nm in diameter. A stiff cantilever was used to get a large indentation force ensuring that the measurement was in the so-called strong-indentation regime and the piezoresponse was dominated by the d_{33} of ZnO films [110].

3 Effects of TM-doping on the local structure and piezoresponse of ZnO films

3.1 V-substitution-induced ferroelectric and enhanced piezoresponse of $Zn_{1-x}V_xO$ films

During the last decade, researchers have observed that doping can induce some anomalous properties in binary compounds with simple structure. For instance, spontaneous polarization were found in doped binary compounds $Pb_{1-x}Ge_xTe$, $Zn_xCd_{1-x}Te$, $Zn_{1-x}Li_xO$, $Zn_{1-x}Mg_xO$, and $Zn_xCd_{1-x}S$ [111–115]. We also observed the ferroelectric behavior in $Zn_{0.975}V_{0.025}O$ films [51]. It is well known that most ferroelectric materials have a strong piezoresponse, and since $Zn_{0.975}V_{0.025}O$ films possess ferroelectricity, it may have a strong piezoresponse. The dependence of piezoelectric displacement on applied voltage was characterized and the typical displacement-applied voltage (*D*-*V*) loop is shown in Figure 1. As is shown, a typical well-shaped *D*-*V* butterfly loop is obtained in the film with a maximum displacement of ~1.1 nm appearing at −8 V. This result displays a strain as high as 0.48% and indicates the ferroelectric behavior of the film.

It is evident that every point on the *D*-*V* loop contains information about the piezoelectric displacement under the applied voltage. Piezoresponse d_{33} can be calculated via the law of converse piezoelectric effect:

$$d_{33}=D/V. \quad (1)$$

The piezoresponse hysteresis loop is obtained by calculating the piezoresponse from the *D*-*V* curve based on eq. (1), as shown in Figure 1, where the piezoresponse hysteresis loop clearly shows that the $Zn_{0.975}V_{0.025}O$ film is switchable and ferroelectricity is retained. A piezoresponse d_{33} value of

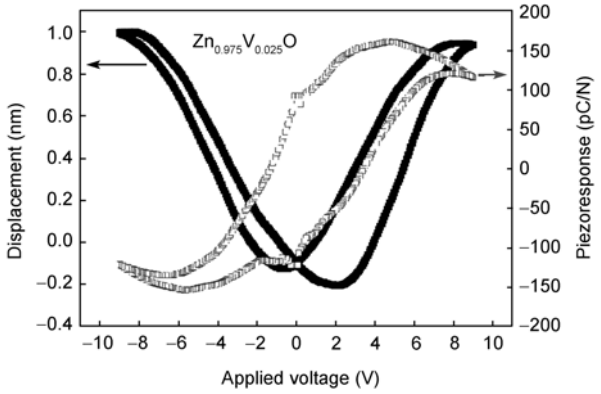

Figure 1 A representative *D*-*V* curve and the piezoresponse hysteresis loop of $Zn_{0.975}V_{0.025}O$ films.

~170 pC/N is also obtained in $Zn_{0.975}V_{0.025}O$ film, which is one order of magnitude larger than that of pure ZnO films.

It is well known that the properties of materials depend on their microstructures. Since the piezoresponse of $Zn_{0.975}V_{0.025}O$ films was enhanced significantly, the microstructure might be improved. Figure 2 displays the microstructure characterization obtained for pure and $Zn_{0.975}V_{0.025}O$ films. From Figure 2(a), only (002) and (004) peaks that reflect ZnO wurtzite structure can be seen in the two patterns, which suggests a strong *c*-axis preferred orientation. Besides, no reflections of V metal and second phases of V were detected, thus the presence of metallic V or clusters of V oxides can be excluded under the detection limit of XRD. The inset of Figure 2(a) shows a comparison of (002) peaks of pure ZnO and $Zn_{0.975}V_{0.025}O$ films. A relative shift to a higher angle can be seen, implying V incorporation into the wurtzite lattice. Generally, when TM ion with ionic size smaller than that of Zn^{2+} substitutes for Zn^{2+} site in ZnO films, (002) peak would shift to a higher angle.

To more clearly observe the microstructure of ZnO films, Figure 2(b) shows the cross-sectional HRTEM image and SAD of $Zn_{0.975}V_{0.025}O$ films. As can been seen, V metal and V-rich clusters are absent throughout the overall film. Energy-dispersive x-ray spectroscopic (EDXS) data taken at a number of locations throughout the specimen reveal a uniform solid solution of V dissolved in ZnO, with V concentration keeping ~2.5 at.%. The inset of Figure 2(b) shows the SAD pattern of the film, which confirms that $Zn_{0.975}V_{0.025}O$ film exhibits perfect preferred orientation. A representative (002) crystal grain marked by two arrows in Figure 2(b) shows that the grain is pillarlike and the diameter is ~16 nm.

XRD and HRTEM characterizations show that V-doping can improve the crystallographic quality of ZnO films, which would enhance the piezoresponse. However, since both pure and doped samples are highly oriented, this effect should be limited. Therefore, there are some intrinsic factors which couple with the piezoresponse strongly inducing the drastic difference.

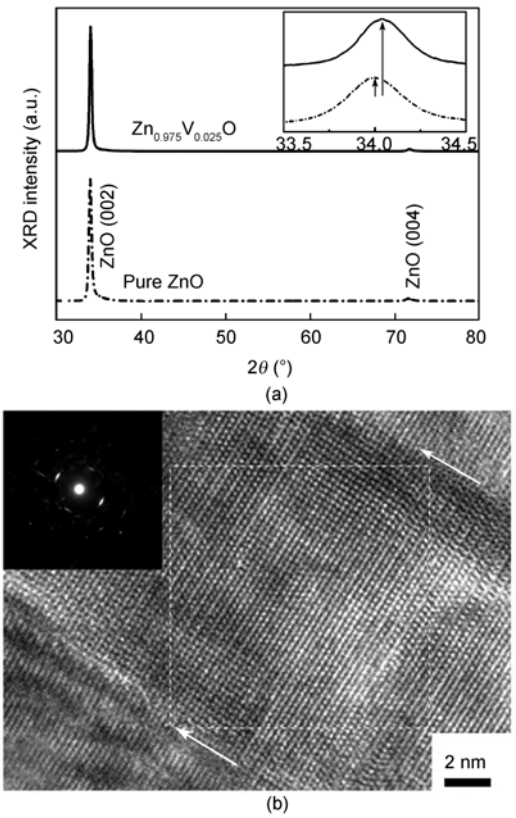

Figure 2 Microstructure characterization of ZnO:V films. (a) XRD patterns of pure ZnO and $Zn_{0.975}V_{0.025}O$ films. The inset shows a comparison of (002) reflections of the two films; (b) HRTEM image of $Zn_{0.975}V_{0.025}O$ films. The inset is the SAD pattern of the films.

In order to seek the origin of the giant piezoresponse, we used V *K*-edge X-ray absorption near-edge structure (XANES) spectrum to investigate the chemical state and local environment of V dopants in the lattice and Figure 3 shows the corresponding absorption spectrum. A distinguishable pre-edge peak (marked 1) can be found in the figure, which is ascribed to a 1s→3d transition. One can also find a main absorption (marked 2), which is due to a 1s →4p transition [116]. Additionally, the spectrum also exhibits a weak shoulder on the low-energy side of the main peak which has been assigned as the 1s→4p shakedown transition [117]. Wong et al. [118] reported that the position of the pre-edge peak varies linearly with the valence state of the absorbing vanadium atom and that the intensity contains information about its local environment. The position of peak 1 is ~5469.8 eV, which indicates a valence state of +5. On the other hand, 1s→3d dipole transitions are strictly forbidden for a site with the inversion symmetry like octahedrally coordinated position. With the symmetry lowering, the intensity increases. A peak, whose intensity is comparable with an edge jump, can be obtained for a tetrahedral coordination. The pre-edge peak in the experimental curve is sharp, indicating that V is tetrahedrally coordinated [119]. Thus, through qualitative analysis of the XANES, we have

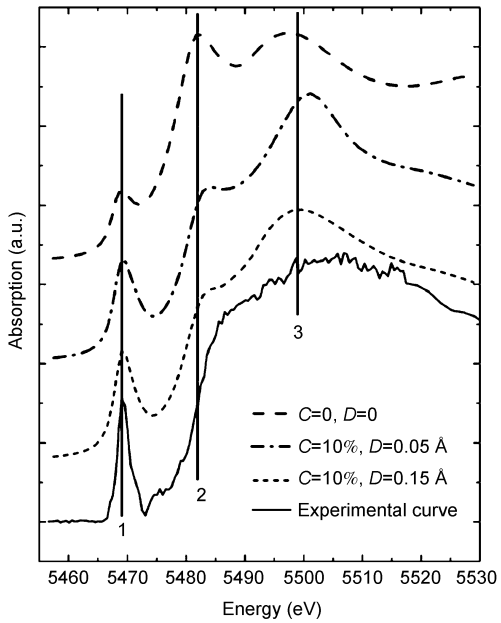

Figure 3 Experimental and calculated V *K*-edge XANES spectra for $Zn_{0.975}V_{0.025}O$ films.

found that V with tetrahedrally coordinate substitutes for Zn^{2+} in 5+ state.

In order to find out the specific site of V^{5+} in ZnO films, V *K*-edge XANES spectra have been calculated via the full multiple-scattering theory using the ab-initio method. As shown in Figure 3, three main features (peaks 1, 2 and 3) match the experimental curve to a certain extent by simply replacing the central Zn by V in a designed V-doped ZnO cluster. However, the relative heights of peaks 2 and 3 are different from those of the experimental spectrum, and there is a much lower pre-edge peak compared to the experimental spectrum. Constriction of local VO_4 units (C) and displacement of V^{5+} ion from the cell center (D) were then introduced as parameters in the calculation. Introduction of VO_4 constriction and V^{5+} displacement improved the similarity of the simulative curve to the experimental curve. When the VO_4 constriction is 10% and V^{5+} displacement is 0.15 Å, the closest simulation is obtained. This accurate replication of the characteristics of the experimental spectrum implies that V^{5+} displacement likely occurs and is responsible for ferroelectricity in the ZnO:V system. It is therefore concluded that V^{5+} ionic displacement is responsible for the ferroelectricity in ZnO:V system.

As discussed above, one can find that switchable spontaneous polarization (P_s), i.e., ferroelectricity emerges in ZnO films because of V-doping. Since pure ZnO is noncentrosymmetric and possesses non-switchable P_s, the addition of V can either modify already existing P_s of ZnO by making it switchable or create additional component of P_s. It is well-known that piezoresponse d_{33} in the ferroelectrics with centrosymmetric paraelectric phase can be expressed as follows [120]:

$$d_{33}= 2Q_{\text{eff}}\varepsilon_0\varepsilon_r P_s, \quad (2)$$

where Q_{eff} is the effective electrostriction coefficient, and ε_0 and ε_r are the permittivity of free space and relative permittivity, respectively. From this equation, one can find that the piezoresponse in ferroelectrics is directly dependent on P_s via a factor linking the electrostrictive characteristics and the dielectric constants. As discussed above, the switchable P_s emerges in ZnO films via V-doping, thus the piezoresponse d_{33} would be enhanced. Moreover, ε_r of the V-doped ZnO films was determined to be in the range of 18–23 by dielectric measurements with respect to ~9 for pure ZnO samples. The improvement of ε_r is considered to be the induce of P_s [121], which also enhances the piezoresponse according to eq. (2). Therefore, from the macroscopic point of view, the giant piezoresponse in ZnO:V films is considered to be the emergence of switchable spontaneous polarization as well as the relatively high permittivity.

From the microscopic point of view, the dominant effect of the electric field in wurtzite semiconductors is to rotate the bonds that are non-collinear with the polar *c*-axis, i.e., Zn2–O1 bonds (see Figure 4), toward the direction of applied field and thus producing strain [122]. And thus the piezoresponse in wurtzite materials is mainly governed by the ease of bond bending and rotation. Similarly, the piezoresponse of V-doped ZnO films is mainly governed by the ease of V–O1 bond bending and rotation. Since V^{5+} ion has a higher positive charge than Zn^{2+} ion and the ionic size of V^{5+} (0.59 Å) is smaller than that of Zn^{2+} (0.74 Å), the non-collinear V–O1 bonds ought to have a stronger polarity than Zn2–O1 bonds and hence can rotate more easily in an applied field, which produces large piezoelectric displacement and enhances corresponding piezoresponse.

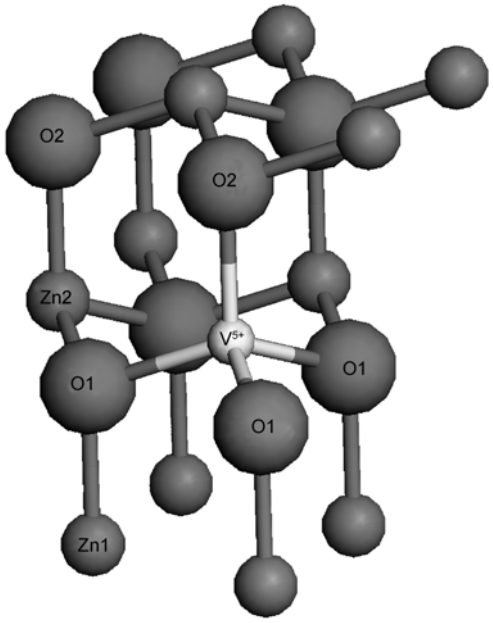

Figure 4 (2×2×1) supercell of V-doped ZnO system.

The piezoresponses of ZnO:V films with various V content have been systematically investigated, as shown in Table 1. The piezoresponses for bulk ZnO and the nanobelts are ~9.9 and ~26.7 pC/N, respectively. The piezoresponse enhanced significantly with V-doping and reaches a peak value of ~170 pC/N, which is about 13 times larger than that of pure ZnO film (11.8 pC/N). The intriguing piezoelectric property means that V-doped ZnO is promising candidates for piezoelectric devices, such as sensors, actuators, transducers and so on. Enhanced piezoresponse is comparable with that of Pb-based piezoelectric materials, thus V-doped ZnO can be considered as potentially alternative to Pb-based piezoelectric materials. Interestingly, the enhanced piezoresponse not only appears in V-doped ZnO films, but also exists in V-doped ZnO nanofibers [123].

3.2 Piezoresponse enhancement in ZnO:Cr films

Cr^{3+} ion has a higher positive charge than Zn^{2+} ion and the ionic size of Cr^{3+} (0.63 Å) is smaller than that of Zn^{2+}, which is similar to V^{5+} ion. Therefore, it is of significance to investigate the effect of Cr-doping on the piezoresponse of ZnO films.

The chemical state and the local environment of the dopants in ZnO lattice are critical for the piezoresponse of doped-ZnO. XPS was used to study the chemical state of Cr in ZnO:Cr films and the corresponding spectra are shown in Figure 5(a). The Zn LMM Auger lines interfere with the more intense Cr $2p_{1/2}$ lines in the XPS spectra. The core level binding energy for Cr $2p_{3/2}$ primary peaks locates at ~577.4 eV, which is very close to the reported binding energy 577.0–577.2 eV of Cr^{3+} states [124], indicating that Cr dopants are incorporated into the ZnO lattice as Cr^{3+} ion. No apparent change in the Cr binding energy is observed with increasing Cr doping content, indicating that the chemical state Cr ion has not changed under the doping-content of 9 at.%.

XANES was used to study the specific local environment of Cr dopants and the normalized Cr *K*-edge absorption spectrum of $Zn_{0.91}Cr_{0.09}O$ film is shown in Figure 5(b). The presence of the pre-edge peak (marked A) implies a tetrahedral environment of the X-ray absorbing transition metals, which coincides well with the fourfold coordination of substitutional Cr atoms in wurtzite ZnO. Comparing the peak

Table 1 Piezoresponses of $Zn_{1-x}V_xO$ films, ZnO bulk and ZnO nanobelts

Sample	d_{33} (pC/N)	Sample	d_{33} (pC/N)
ZnO bulk	9.9	$Zn_{0.99}V_{0.01}O$	12.3
Oriented ZnO film	12.4	$Zn_{0.985}V_{0.015}O$	56
ZnO nanobelts	26.7	$Zn_{0.98}V_{0.02}O$	82
Pure ZnO film	11.8	$Zn_{0.975}V_{0.025}O$	170
$Zn_{0.995}V_{0.005}O$	12	$Zn_{0.97}V_{0.03}O$	95

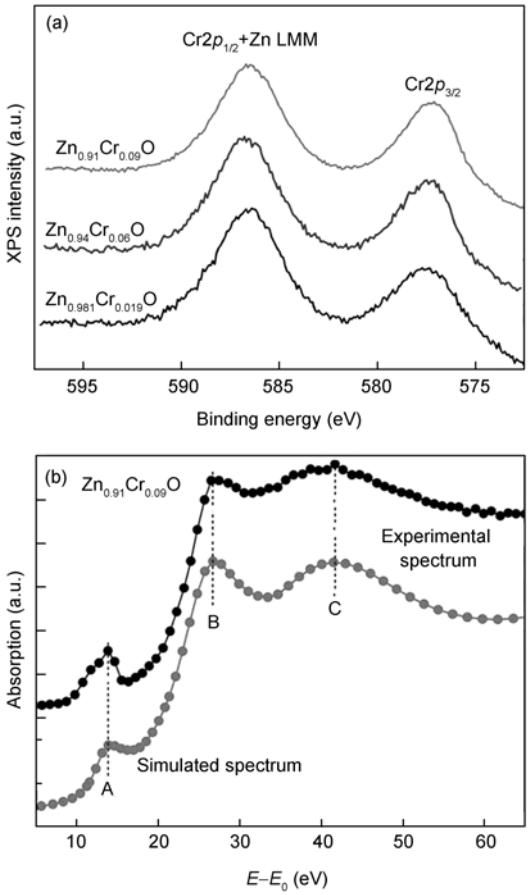

Figure 5 Chemical state and local environment charatcterization of Cr-dopant. (a) Cr 2*p* core level regions of $Zn_{0.981}Cr_{0.019}O$, $Zn_{0.94}Cr_{0.06}O$ and $Zn_{0.91}Cr_{0.09}O$ films; (b) experimental and simulated Cr *K*-edge XANES spectra of $Zn_{0.91}Cr_{0.09}O$ film.

numbers and positions, the absorption spectrum of $Zn_{0.91}Cr_{0.09}O$ film is different from those of Cr, Cr_2O_3, CrO_2, and CrO_3 [125], indicating that Cr dopants do not exist as metal or oxide clusters. Cr *K*-edge XANES spectra have been calculated via the full multiple-scattering theory using ab initio method, in which Cr dopants are modeled as Cr^{3+} to substitute for Zn^{2+} site [126]. Comparing the experiment and calculated spectra, one can find that the three feature peaks are fitted very well, revealing that Cr^{3+} indeed substitutes for the Zn^{2+} site.

The dependence of piezoelectric displacement on the applied voltage was measured and the corresponding *D*-*V* loop is shown in Figure 6. One can see that a typical *D*-*V* butterfly curve is obtained with a maximum displacement of ~0.9 nm appearing at –9 V. This result displays a strain as high as 0.6% and indicates the ferroelectric behavior of the films. The piezoresponse-applied voltage loop calculated from the *D*-*V* curve based on the law of converse piezoelectric effect clearly shows that the $Zn_{0.94}Cr_{0.06}O$ film is switchable and ferroelectricity is retained. This phenomenon is similar to that previously observed in V-doped ZnO films. The relative permittivity of $Zn_{0.94}Cr_{0.06}O$ film is also

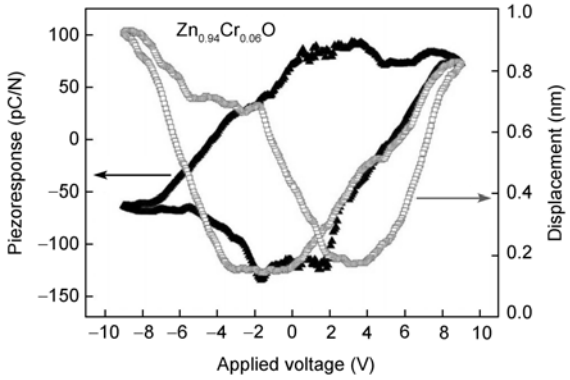

Figure 6 A representative *D-V* curve and the piezoresponse hysteresis loop of $Zn_{0.94}Cr_{0.06}O$ films.

alike, which is determined to be ~18 by dielectric measurements with respect to ~9 for pure ZnO films. Thus, from the macroscopic point of view, the maximum piezoresponse value of 120 pC/N in $Zn_{0.94}Cr_{0.06}O$ film arises from the higher relative permittivity and the emergence of P_s in ZnO films due to Cr-doping. From the microscopic point of view, Cr^{3+} with smaller ionic size and higher positive charge substitutes for Zn^{2+} site in ZnO:Cr films, which makes the non-collinear Cr–O1 bonds rotate more easily to the applied field than Zn2–O1 bonds, producing large piezoelectric displacement and enhanced piezoresponse.

3.3 Effects of Mn content on the piezoresponse of ZnO:Mn films

So far, we have obtained $Zn_{0.975}V_{0.025}O$ and $Zn_{0.94}Cr_{0.06}O$ films with piezoresponse values of ~170 and ~120 pC/N, respectively, which are more than ten times larger than that of pure ZnO films. The piezoresponses of these doped-ZnO films are comparable with that of lead-free piezoelectric ceramics, such as bismuth sodium titanate and alkali niobates, which have been widely studied in the last few decades. However, we also found that 2 at.% Cu-doped ZnO films have a piezoresponses of ~13.6 pC/N, and that Fe- and Co-doped ZnO films with the same doping concentration have piezoresponses values of ~6 pC/N and ~11 pC/N, respectively. Thereby, a question emerges immediately: Why can ZnO films doped with moderate V, Cr and Cu have enhanced piezoresponses values whereas ZnO films doped with 2 at.% Fe and Co have decreased piezoresponses. There are two possibilities, one is that only some dopants like V, Cr, and Cu could improve the piezoresponse of ZnO, while other elements like Fe, Co would decrease its piezoresponse; the other is that there is a general rule describing the impact of doping on the piezoresponse of ZnO films. To answer this question, ZnO:Mn films with various Mn-doping content were investigated.

The piezoresponses of $Zn_{1-x}Mn_xO$ are presented in Table 2. One can find that the piezoresponses of $Zn_{0.978}Mn_{0.022}O$ and $Zn_{0.952}Mn_{0.048}O$ films are smaller than that of pure ZnO film. When $x > 4.8$ at%, the piezoresponse increases rapidly with increasing x. The maximum piezoresponse value of ~86 pC/N is obtained in $Zn_{0.913}Mn_{0.087}O$ film, which is comparable to some lead-free piezoelectric materials and can be considered as a lead-free and biocompatible piezoelectric material. As x exceeds 8.7 at%, the piezoresponse decreases, which may result from structural deterioration by over-doping, but the value is still much greater than that of pure ZnO fims.

Table 2 Piezoresponses of $Zn_{1-x}Mn_xO$ films

Sample	d_{33} (pC/N)	Sample	d_{33} (pC/N)
Pure ZnO film	12.1	$Zn_{0.913}Mn_{0.087}O$	86
$Zn_{0.978}Mn_{0.022}O$	10.5	$Zn_{0.895}Mn_{0.105}O$	72
$Zn_{0.952}Mn_{0.048}O$	8.2	$Zn_{0.88}Mn_{0.12}O$	53
$Zn_{0.931}Mn_{0.069}O$	38		

To study the macroscopic reasons of piezoresponse difference among $Zn_{1-x}Mn_xO$ films, the *D-V* curves and the corresponding piezoresponse-applied voltage loops were measured, as shown in Figure 7. As can be seen, the typical *D-V* butterfly loop can be found in Figures 7(b) and (c), which indicates that P_s emerges in $Zn_{0.931}Mn_{0.069}O$ and $Zn_{0.913}Mn_{0.087}O$ films, and the corresponding permittivity would be higher in both films, which results in the enhancement of piezoresponses according to eq. (2). However, the typical *D-V* butterfly loop is absent in $Zn_{0.952}Mn_{0.048}O$ films as shown in Figure 7(a) and the maximum displacement is less than 0.16 nm, which indicates a small piezoresponse.

To investigate the influence of Mn content on the piezoresponse of Mn-doped ZnO films from a microscopic point of view, Mn L_3-edge XAS spectra were measured, which are shown in Figure 8. It is known that the XAS at the Mn L_3-edge determines the 3d occupancy of Mn ion and hence provides the valence states of Mn ion [127]. As the chemical state changes from Mn^{2+} to Mn^{3+} and Mn^{4+}, the L_3-edge shifts toward higher energy and the spectral shape changes significantly. As shown in the figure, all the samples exhibit multiple absorption peaks between 640 eV and 646 eV, excluding the possibility of Mn impurities which does not display multiple structures [128]. A distinct XAS fingerprint of divalent Mn ion appears in $Zn_{0.952}Mn_{0.048}O$ films, which indicates that the chemical state of Mn in $Zn_{0.952}Mn_{0.048}O$ films is Mn^{2+}. However, as for $Zn_{1-x}Mn_xO$ (x = 6.9 at% and 8.7 at%) films, the XAS L_3-edge shifts to higher energy and the line shape changes significantly, which is attributed to the existence of mixed valence states of Mn^{3+} and Mn^{4+} [129]. Using the crystal field symmetry to investigate the local environment of Mn in all films carefully, we found that Mn^{2+} substitutes for Zn^{2+} when $x \leqslant 4.8$ at% and the mixed valence states of Mn^{3+}/Mn^{4+} substitutes for Zn^{2+} when $x \geqslant 6.9$ at%.

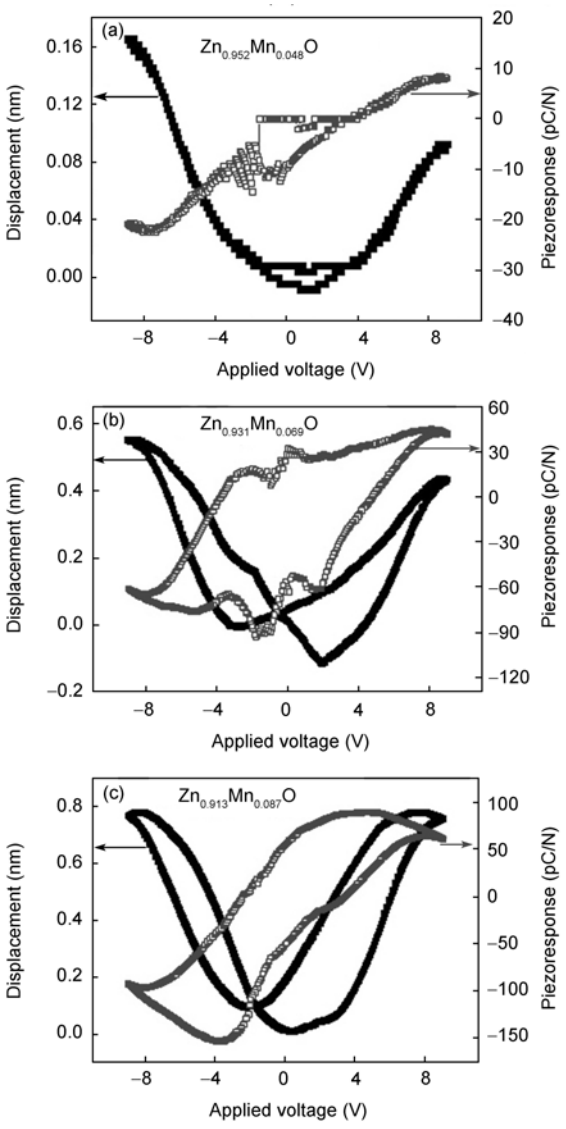

Figure 7 *D-V* curves and the corresponding piezoresponse loops of $Zn_{1-x}Mn_xO$ films. (a) $Zn_{0.952}Mn_{0.048}O$; (b) $Zn_{0.931}Mn_{0.069}O$; (c) $Zn_{0.913}Mn_{0.087}O$.

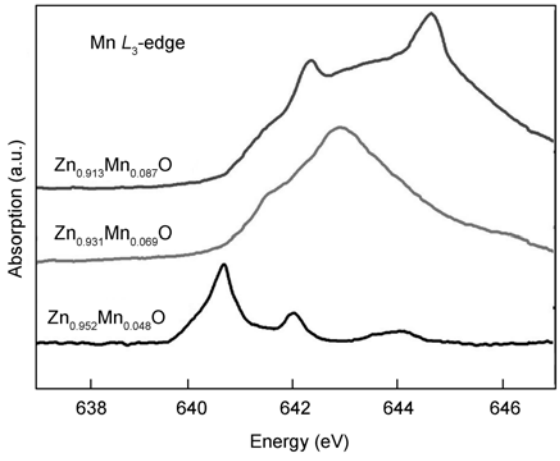

Figure 8 Room-temperature XAS spectra near Mn L_3-edges of $Zn_{1-x}Mn_xO$ films (x = 4.8 at%, 6.9 at%, 8.7 at%).

The piezoresponse of Mn-doped ZnO films is mainly governed by the ease of Mn–O1 bond bending and rotation. When $x \geqslant 6.9$ at%, Mn substitutes Zn as Mn^{3+}/Mn^{4+} and the ionic radius of Mn^{3+}/Mn^{4+} (0.66 Å/0.60 Å) is smaller than that of Zn^{2+} (0.74 Å), which makes the Mn–O1 bonds switch toward the applied field direction conveniently. Moreover, Mn^{3+}/Mn^{4+} have higher positive charge than Zn^{2+} ion and the noncollinear Mn–O1 bonds have stronger polarity than Zn2–O1 ones. Hereby, Mn–O1 bonds can rotate more easily under applied field than Zn2–O1 ones, which results in large piezoelectric displacement and the corresponding piezoresponse enhances. However, when $x > 8.7$ at%, the crystal quality is deteriorated greatly by Mn overdoping, and thus d_{33} decreases. On the other hand, Mn substitutes Zn as Mn^{2+} when $x \leqslant 4.8$ at% and the ionic radius of Mn^{2+} (0.80 Å) is larger than that of Zn^{2+}, which makes the rotation of Mn^{2+}–O1 bonds more difficult than that of Zn2–O1, and thus the piezoresponse is smaller than that of undoped ZnO films.

Therefore, we not only obtained $Zn_{0.913}Mn_{0.087}O$ films with enhanced piezoresponse, but also obtained $Zn_{0.952}Mn_{0.048}O$ films with decreased piezoresponse. Thus, the first possibility can be precluded and there is a general rule describing the impact of doping on the piezoresponse of ZnO films.

4 General rule describing the impact of doping on the piezoresponse of ZnO films

So far, we have investigated various TM-doped ZnO films (TM = Fe, Co, Cu, V, Cr and Mn), Table 3 shows the parameters of dopants and the corresponding piezoresponses of TM-doped ZnO films. As shown by the table, V is in +5 oxidation state in $Zn_{0.975}V_{0.025}O$ and Cr is in +3 oxidation state in $Zn_{0.94}Cr_{0.06}O$. The ionic size of both V^{5+} and Cr^{3+} is smaller than that of Zn^{2+}, and the corresponding piezoresponse are more than ten times larger than that of pure ZnO films. In corresponding TM-doped ZnO, Cu, Fe, and Co exist at the chemical state of +2. The sizes of Fe^{2+} and Co^{2+} are bigger than that of Zn^{2+} but Cu^{2+} is a little smaller, and the piezoresponse of Fe- and Co-doped ZnO films are smaller than that of pure ZnO films while the piezoresponse of Cu-doped ZnO films is a little bigger than that of pure ZnO films. In Mn-doped ZnO films, when Mn^{2+} with bigger ionic size substitutes for Zn^{2+} site, the piezoresponse is smaller than that of pure ZnO films, while Mn^{3+}/Mn^{4+} with higher positive charge and smaller ionic size substitutes for Zn^{2+} site, the piezoresponse is much higher than that of pure ZnO films. Therefore, via studying the relationship between dopant ionic size and the piezoresponse values, we proposed a general rule describing the impact of doping on the piezoresponse of ZnO films. That is, when the doped ion substitutes for Zn^{2+} site, ZnO doped with a small ion produces enhanced piezoresponse whereas ZnO doped with a big ion results in a decreased piezoresponse. This general

Table 3 The parameters of dopants and corresponding piezoresponses of TM-doped ZnO films

Dopant	Doping content (at.%)	Chemical state	Ionic size (Å)	d_{33} (pC/N)
Fe	2	Fe^{2+} substitutes for Zn^{2+}	0.76	6
Co	2	Co^{2+} substitutes for Zn^{2+}	0.79	11
Mn	4.8	Mn^{2+} substitutes for Zn^{2+}	0.80	8.2
Mn	8.7	Mn^{3+}/Mn^{4+} substitutes for Zn^{2+}	0.66/0.60	86
V	2.5	V^{5+} substitutes for Zn^{2+}	0.59	170
Cr	6	Cr^{3+} substitutes for Zn^{2+}	0.63	120
Cu	2	Cu^{2+} substitutes for Zn^{2+}	0.72	13.6

rule, if correct, would be useful for guiding the design of new semiconductors with enhanced electromechanical responses. The chemical state of Fe in Fe-doped ZnO can be different on different conditions and Fe ionic size can be changed with the change of its chemical state in ZnO:Fe [130, 131]. Therefore, we used various Fe-doping contents and the annealing treatments to verify this rule.

The structural characterization indicates that the crystal quality of $Zn_{0.974}Fe_{0.026}O$ films is similar to that of $Zn_{0.988}Fe_{0.012}O$ films, while their piezoresponses are of tremendous difference. The *D-V* curve and the corresponding piezoresponse loops of $Zn_{0.988}Fe_{0.012}O$ film are shown in Figure 9. From Figure 9, one can find that the film has a typical well-shaped *D-V* butterfly loop with a displacement maximum of ~1.25 nm appearing at −8.9 V. The corresponding piezoresponse loop clearly shows that the $Zn_{0.988}Fe_{0.012}O$ film is switchable and ferroelectricity is retained. A giant piezoresponse as high as of 200 pC/N can be found in Figure 9. Based on eq. (2), the macroscopic origin of the giant piezoresponse is the emergence of P_s and the corresponding high permittivity in $Zn_{0.988}Fe_{0.012}O$ films. Figure 10 shows the *D-V* curve and corresponding piezoresponse loops of $Zn_{0.974}Fe_{0.026}O$ films. It is found that the typical butterfly loop is not observed in the figure and the maximum displacement is less than 0.04 nm. The piezoresponse of $Zn_{0.974}Fe_{0.026}O$ films is 7 pC/N, which is smaller than that of undoped ZnO films. From the XPS and XAS results, it is found that Fe^{3+} ion substitutes for Zn^{2+} in $Zn_{0.988}Fe_{0.012}O$ films, and the ionic size of Fe^{3+} (0.64 Å) is smaller than that of Zn^{2+}, which makes the switch of the Fe^{3+}-O1 bond toward the applied field direction convenient. Moreover, Fe^{3+} has a higher positive charge than Zn^{2+} ion and noncollinear Fe^{3+}-O1 bonds have a stronger polarity than Zn2-O1 ones. Hence, Fe^{3+}-O1 bonds can rotate more easily under an applied field than Zn2-O1 ones, which produces large piezoelectric displacement and enhances the piezoresponse. Whereas, Fe^{2+} ion substitutes for Zn^{2+} in $Zn_{0.974}Fe_{0.026}O$ films and the ionic size of Fe^{2+} (0.76 Å) is larger than that of Zn^{2+}, which makes the rotation of Fe^{2+}-O1 bonds become more difficult than that of Zn2-O1. And the piezoelectric displacement is small and the corresponding piezoresponse is smaller than that of pure ZnO films.

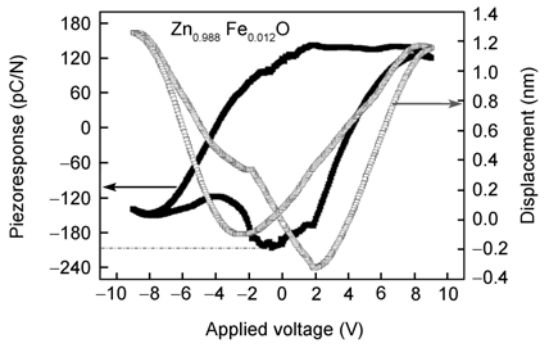

Figure 9 *D-V* loop and corresponding piezoresponse curve of $Zn_{0.988}Fe_{0.012}O$ film.

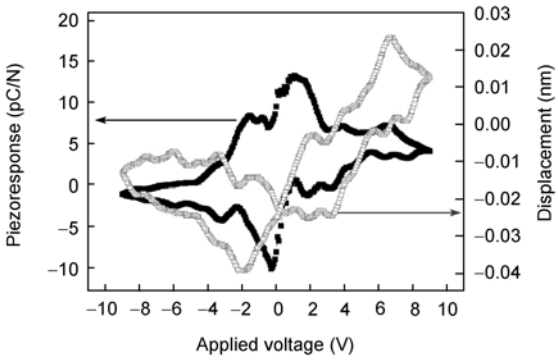

Figure 10 *D-V* loop and corresponding piezoresponse curve of $Zn_{0.974}Fe_{0.026}O$ films.

An interesting question is emerged: How would the piezoresponse of ZnO:Fe films be changed if the valence and the ionic size of Fe dopant in ZnO films change? Hereby, we modulated Fe chemical states and ionic sizes in $Zn_{1-x}Fe_xO$ (x=0, 1.2, and 2.6 at.%) films by a series of post-annealing treatments. After the post-annealing, the piezoresponses of all the samples were measured and the corresponding values were shown in Table 4.

Although the piezoresponses of all the samples are improved after annealing in O_2 environment, the increase in the piezoresponse of $Zn_{0.974}Fe_{0.026}O$ is remarkable. Post-annealing may improve the crystallographic quality and thus enhance the piezoresponse. Since both pure ZnO and $Zn_{0.974}Fe_{0.026}O$ films are in the same annealing condition,

Table 4 The changes of piezoresponses (pC/N) after a series of post-treatments

Post-treatment	Pure ZnO	$Zn_{0.988}Fe_{0.012}O$	$Zn_{0.974}Fe_{0.026}O$
As deposited	11.6	127	7
O_2 annealed	12.1	128	120
H_2 annealed	11.8	9	7

this effect should be the same for pure ZnO and $Zn_{0.974}Fe_{0.026}O$ films. However, the piezoresponse of $Zn_{0.974}Fe_{0.026}O$ (120 pC/N) is one order of magnitude larger than that of undoped ZnO (12.1 pC/N). Therefore, the tremendous improvement in the piezoresponse of $Zn_{0.974}Fe_{0.026}O$ seems to result from some intrinsic factor except for the crystallographic quality improvement. The *D*-*V* loop of $Zn_{0.974}Fe_{0.026}O$ films after annealing in O_2 environment is shown in Figure 11. A typical well-shaped *D*-*V* butterfly loop can be seen, indicating the ferroelectric behavior of the $Zn_{0.974}Fe_{0.026}O$ film. Therefore, the tremendous improvement of piezoresponse can be ascribed to switchable spontaneous polarizations and the accompanying high permittivities.

XAS was used to investigate the changes in the chemical state and ionic size of Fe in the $Zn_{0.974}Fe_{0.026}O$ film after O_2 annealing, and the corresponding Fe $L_{2,3}$-edge XAS spectra are shown in Figure 12. The two Fe $L_{2,3}$ line shapes are consistent with a tetrahedral coordination, as expected of Fe ion substituting for Zn in the ZnO [132]. However, the XAS spectra of $Zn_{0.974}Fe_{0.026}O$ before and after O_2 annealing are different, indicating the different chemical states of Fe ion. Fe L_2 and L_3 edges of $Zn_{0.974}Fe_{0.026}O$ films as deposited are located at ~708 eV and ~720 eV, respectively, and the line shape and *L*-edge peak position are coincident with those of Fe^{2+} [133, 134], indicating that Fe has a +2 oxidation state in $Zn_{0.974}Fe_{0.026}O$ films. After O_2 annealing, the film shows a dominant peak near 710 eV, accompanied by double peaks near 721 and 723 eV, which are characteristic of Fe^{3+} ion [135]. Therefore, the dominant chemical state of Fe ion changes from Fe^{2+} to Fe^{3+} after O_2 annealing. Fe^{3+} ion has a smaller ionic size and higher positive charge, and thus Fe^{3+}-O1 bonds can rotate more easily under an applied field than Zn_2-O_1 ones, which produces large piezoelectric displacement and the piezoresponse enhanced.

On the other hand, the piezoresponse of $Zn_{0.988}Fe_{0.012}O$ films decreases dramatically after H_2 annealing as shown in Table 4. XPS was used to study the changes of Fe chemical state and ionic size in $Zn_{0.988}Fe_{0.012}O$ film after H_2 annealing, and the corresponding Fe 2*p* XPS spectra are shown in Figure 13. Fe $2p_{1/2}$ and $2p_{3/2}$ peaks in $Zn_{0.988}Fe_{0.012}O$ films as deposited are located at 724.7 eV and 710.6 eV, respectively, which are similar to the values reported for Fe_2O_3:Fe $2p_{1/2}$ at 724.9 eV and Fe $2p_{3/2}$ at 710.7 eV [136]. The spectrum shows a shake-up contribution at about 718.6 eV, which indicates that Fe has a +3 oxidation state [137]. After H_2 annealing, Fe $2p_{3/2}$ and $2p_{1/2}$ signals of the films are centered at 709.6 eV and 722.7 eV, respectively, which are very close to those of Fe^{2+} (709.30 eV for Fe $2p_{3/2}$ and 722.3 eV for Fe $2p_{1/2}$) [138]. Therefore, the dominant chemical state of Fe ion in $Zn_{0.988}Fe_{0.012}O$ films changes from Fe^{3+} to Fe^{2+} after H_2 annealing. The ionic size of Fe^{2+} ion is bigger than that of Zn^{2+}, and thus it is more difficult for Fe^{2+}-O1 bonds

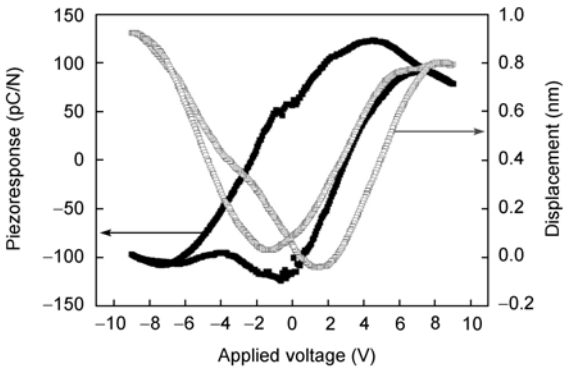

Figure 11 *D*-*V* loop and corresponding piezoresponse curve of $Zn_{0.974}Fe_{0.026}O$ films after O_2 annealing.

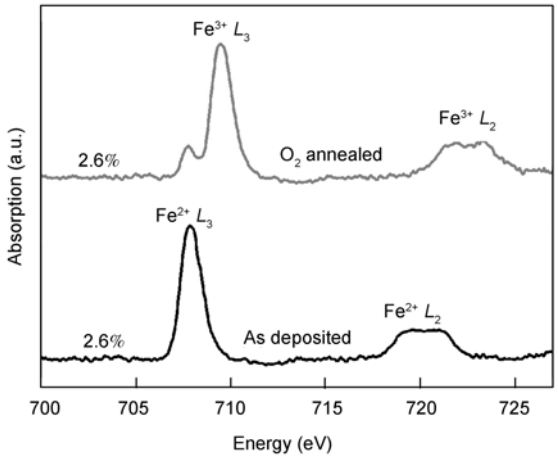

Figure 12 Room-temperature XAS spectra near Fe $L_{2,3}$ edges of $Zn_{0.974}Fe_{0.026}O$ films as deposited and after O_2 annealing.

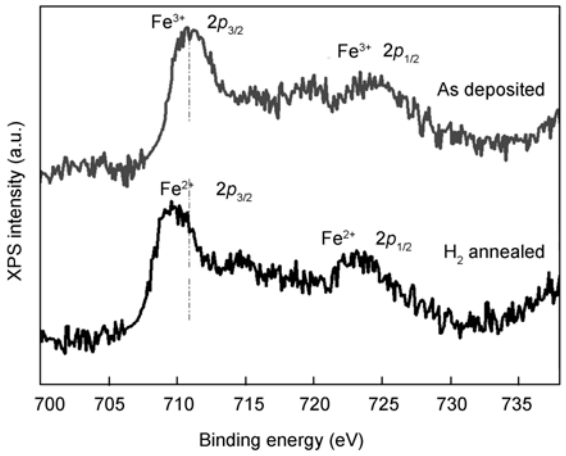

Figure 13 Fe 2*p* XPS spectra of $Zn_{0.988}Fe_{0.012}O$ films as deposited and after H_2 annealing.

to rotate to the applied field than Zn_2-O_1 ones. And the piezoelectric displacement is small, resulting in the decrease of the piezoresponse.

Through investigating Fe-doped ZnO films and the post-annealing, we verified that the piezoresponse of doped-ZnO films depends on the ionic size and the positive charge of the dopant. When smaller ions substitute for Zn^{2+} in ZnO, they can enhance the piezoresponse, and when bigger ions substitute for Zn^{2+} in ZnO, the piezoresponse can decrease. This general rule can be used for guiding the design of new wurtzite semiconductors with enhanced piezoresponses. Besides, the enhanced piezoresponse of doped-ZnO is comparable with that of widely studied lead-free piezoelectric ceramics. Furthermore, ZnO is structurally simple and easy to fabricate; it is safe and nontoxic and compatible with the semiconductor process. Therefore, doped ZnO with enhanced piezoresponse can be used as a new type of environmental friendly lead-free piezoelectric materials. And the general rule proposes a new way for seeking lead-free piezoelectric materials.

5 TM-doped ZnO based piezoelectric devices

Because of its advantages, especially the excellent piezoelectricity, ZnO thin film has been widely used in industrial piezoelectric devices, such as actuators, resonators, oscillator, SAW and BAW devices. The performances of piezoelectric device strongly depend on the properties of ZnO films. So far, some researchers have fabricated various TM-doped ZnO based piezoelectric devices and reported the performances of these devices.

5.1 Filtering performance improvement in ZnO:V/diamond surface acoustic wave filters

SAW devices have been widely used in communication systems and sensors [139, 140]. The rapid development of high-speed and large-volume communication systems has increased the demand of high-frequency filters with low-loss and high piezoelectric coupling coefficient K^2 [71, 141, 142]. Piezoresponse is the key property to determine the insertion loss and K^2 of ZnO based SAW filters. We used ZnO:V films with enhanced piezoresponse as the piezoelectric material to fabricate high frequency diamond SAW filters and undoped ZnO films were used as contrastive device [143].

Interdigital transducers (IDTs) with the width and space of 600 nm was fabricated using electron-beam lithography (EBL) followed by reactive ion etching (RIE) process. Figure 14(a) shows the SEM photograph of the whole IDTs configuration. It is found that fine IDTs patterns were formed on ZnO/diamond layered structure. Figure 14(b) shows the atomic force microscopy (AFM) characterizations of IDTs patterned on the layered structure. As is shown, IDTs fingers have sharp edges, regular thicknesses of 80 nm and regular width of approximately 600 nm. The IDTs on both undoped and ZnO:V films had the same structure and were developed under the same conditions, thus the different performance of the devices should result from the piezoelectric materials.

Table 5 shows the filtering performance parameters of both kinds of devices. One can find that the K^2 value of ZnO:V devices is on the order of 2.9%, which is higher than that of undoped ZnO devices of 1.6%. ZnO:V films possess a piezoresponse of 115 pC/N, which is one order of magnitude higher than that of undoped ZnO films (11.3 pC/N). Therefore, the efficiency of the energy conversion from the electric RF signal into the SAW would be higher, and the K^2 value for ZnO:V films would be higher.

Besides, the insertion loss of ZnO:V film device is smaller than that of undoped ZnO film device. The K^2 of ZnO:V filters is higher, so the energy loss would be lower. Moreover, ZnO:V films possess better crystallinity and smoother surface than undoped ZnO films, thus the loss caused by piezoelectric materials is lower and correspondingly the

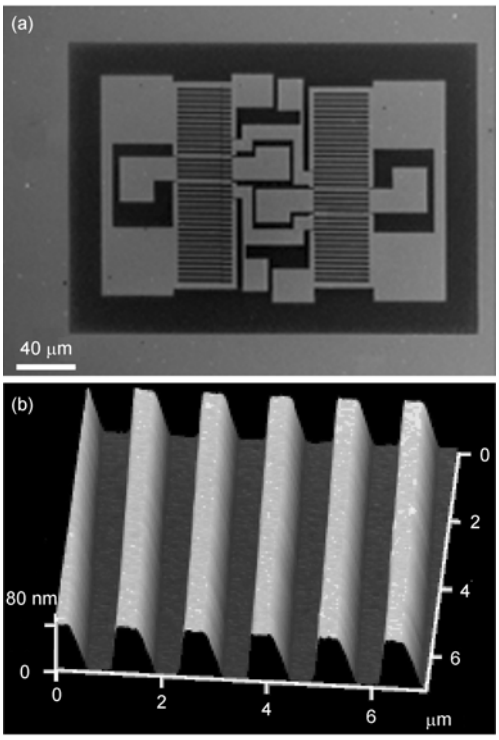

Figure 14 Images of IDTs fabricated on the layered structure (a) SEM photograph of the whole IDTs (b) AFM image of partial IDTs.

Table 5 Filtering performance parameters of the two kinds of devices

Device	K^2	Insertion loss (dB)	Central frequency (GHz)	d_{33} (pC/N)
Pure ZnO device	1.6%	31.6	4.16	11.3
ZnO:V device	2.9%	20.8	4.16	115

insertion loss of the device is lower. Hereby, ZnO:V films are more preferable for the SAW filters. Besides SAW filters, we suggest that the improved properties of V-doped ZnO could also make it a promising candidate for sensors, actuators, and transducers.

5.2 ZnO:Mg based piezoelectric devices

Comparing with ZnO, MgO has higher longitudinal and transverse acoustic velocities. Although MgO is a non-piezoelectric material, $Zn_{1-x}Mg_xO$ crystal retains the wurtzite structure and possesses piezoelectricity for the range of Mg composition below approximately 35% [144]. It is reported that the acoustic velocity increases whereas the K^2 decreases with increasing Mg content in piezoelectric $Zn_{1-x}Mg_xO$ films [145]. Therefore, SAW properties can be tailored by controlling Mg content, or using ZnO/$Zn_{1-x}Mg_xO$ multilayer structures. This tailor technology increases the design flexibility of the low-loss and high frequency SAW devices. Since the $Zn_{1-x}Mg_xO$ is wide bandgap semiconductor and the SAW properties can be tailored, it is a new piezoelectric material for making novel integrated acoustic-optic and acoustic-electronic devices [146].

Walter et al. used $Zn_{1-x}Mg_xO$ to fabricate Love wave filter on ST-cut quartz. They pointed out that K^2 does not decay when Mg content is small and temperature coefficient of frequency (TCF) declines from +30 to +0.44 ppm/°C at 1.5 mol% Mg-doped ZnO films [147]. Chang et al. [85, 148] used $Zn_{1-x}Mg_xO$ to fabricate Love wave sensor. They found that small Mg-doping content would produce a small crystallite size and a rough surface which increase the phase shift, i.e. sensitivity, of the Love wave sensor. However, high Mg-doping content produces too much rough surface which inhibits the propagation of the Love wave and makes the sensitivity decrease instead. Therefore, it is promising to obtain the high sensitivity of Love wave devices for sensing applications based on $Zn_{1-x}Mg_xO$ by adjusting Mg content.

5.3 Other metal-doped ZnO based piezoelectric devices

Some other metals, such as Ni, Cu and Ca, were also used as dopants in ZnO, and the corresponding doped ZnO based piezoelectric devices were reported. Ni-doped ZnO film has high resistivity of over $10^8\,\Omega$ cm [149], which is preferable for fabricating high frequency SAW filters with low insertion loss and high stability. It is reported that the preferable Ni content is between 1 and 2 wt%. Lee et al. have fabricated SAW devices on Cu-doped ZnO films and they pointed out that the devices using Cu-doped ZnO films have higher K^2 and lower insertion loss compared with those devices using undoped films [150]. Such performance improvement of the devices is considered to be related to the desirable *c*-axis preferred orientation and high electrical resistivity in ZnO:Cu films. Water et al. reported that the sensitivity of ZnO based Love wave sensor increases with doping of moderate content of Ca due to the increase of surface roughness [151]. However, the K^2 decreases due to the disordering of crystalline structure and radiation loss from the rough surface. Therefore, via controlling Ca content, one can obtain a suitable ZnO guiding layer for Love wave sensor applications.

6 Conclusions and outlook

In conclusion, ZnO is modified by TM-doping and through choosing appropriate TM-dopant with moderate doping content. It is found that the piezoresponse of ZnO can be enhanced dramatically. The tremendous piezoresponse of doped ZnO films is due to the emergence of P_s and the corresponding high ε_r from the macroscopic point of view. And the microscopic origin of the giant piezoresponse is that the doped ion with smaller ionic size substitutes for Zn^{2+}, which produces large piezoelectric displacement under the applied field and improves the corresponding piezoresponse significantly. The performances of ZnO based piezoelectric devices can be tailored by doping, and TM-doped ZnO is promising for the application of piezoelectric devices. We also put forward a general rule describing the impact of doping on the piezoresponse of ZnO films. That is, when the doped ion substitutes for Zn^{2+} site, doping ZnO with a small ion produces enhanced piezoresponse whereas doping ZnO with a big ion results in decreased piezoresponse. This rule is useful for guiding the design of new wurtzite semiconductors with enhanced piezoresponses. ZnO is structurally simple and easy to fabricate; it is safe and nontoxic and compatible with the semiconductor process. Therefore, doped ZnO with enhanced piezoresponse can be used as a new type of environmental friendly lead-free piezoelectric materials. And the general rule proposes a new way for seeking lead-free piezoelectric materials. The giant piezoresponse could also make TM-doped ZnO a promising candidate for piezoelectric devices, such as sensors, actuators, and transducers. The SAW devices fabricated on TM-doped ZnO films possess low insertion loss and a large K^2, which is preferable for fabricating SAW devices with high frequency and high performance.

We acknowledge the cooperation of Dr. YAN W.S. and HE B. of the National Synchrotron Radiation Laboratory in local structure measurements. We also thank TAI R.Z of Shanghai Synchrotron Radiation Facility (SSRF) and XIE Y.N. of Beijing Synchrotron Radiation Facility (BSRF) for local structure and the chemical state measurements. This work was supported by the National Hi-tech (R&D) Program of China (Grant Nos. 2007AA03Z426 and 2009AA034001), the National Natural Science Foundation of China (Grant Nos. 50871060 and 50772055), and the National Basic Research Program of China (Grant No. 2010CB832905).

1 Bilgen O, Karami M A, Inman D J, et al. The actuation characterization of cantilevered unimorph beams with single crystal piezoelectric materials. Smart Mater Struct, 2011, 20: 0550245

2 Xie J, Mane X P, Green C W, et al. Performance of thin piezoelectric materials for pyroelectric energy harvesting. J Intel Mat Syst Str, 2010, 21(3): 243–249
3 Kholkin A L, Bdikin I K, Kiselev D A, et al. Nanoscale characterization of polycrystalline ferroelectric materials for piezoelectric applications. J Electroceram, 2007, 19(1): 83–96
4 Polla D L, Francis L F. Processing and characterization of piezoelectric materials and integration into microelectromechanical systems. Annu Rev Mater Res, 1998, 28: 563–597
5 Sahoo B, Jaleel V A, Panda P K. Development of PZT powders by wet chemical method and fabrication of multilayered stacks/actuators. Mat Sci Eng B-Solid, 2006, 126(1): 80–85
6 Izyumskaya N, Alivov Y, Cho S J, et al. Processing, structure, properties, and applications of PZT thin films. Crit Rev Solid State, 2007, 32(3-4): 111–202
7 Aksel E, Jones J L. Advances in lead-free piezoelectric materials for sensors and actuators. Sensors, 2010, 10(3): 1935–1954
8 Panda P K. Review: Environmental friendly lead-free piezoelectric materials. J Mater Sci, 2009, 44(19): 5049–5062
9 Li Y, Moon K S, Wong C P. Electronics without lead. Science, 2005, 308(5727): 1419–1420
10 Shimamura K, Takeda H, Kohno T, et al. Growth and characterization of lanthanum gallium silicate $La_3Ga_5SiO_{14}$ single crystals for piezoelectric applications. J Cryst Growth, 1996, 163(4): 388–392
11 Li Y M, Chen W, Zhou J, et al. Dielectric and piezoelecrtic properties of lead-free $(Na_{0.5}Bi_{0.5})TiO_3$-$NaNbO_3$ ceramics. Mat Sci Eng B-Solid, 2004, 112(1): 5–9
12 Ringgaard E, Wurlitzer T. Lead-free piezoceramics based on alkali niobates. J Eur Ceram Soc, 2005, 25(12): 2701–2706
13 Makiuchi Y, Aoyagi R, Hiruma Y, et al. $(Bi_{0.5}Na_{0.5})TiO_3$-$(Bi_{0.5}K_{0.5})TiO_3$-$BaTiO_3$-based lead-free piezoelectric ceramics. Jpn J Appl Phys, 2005, 44(6B): 4350–4353
14 Takenaka T, Nagata H. Current status and prospects of lead-free piezoelectric ceramics. J Eur Ceram Soc, 2005, 25(12): 2693–2700
15 Dalcorso A, Posternak M, Resta R, et al. AB-Initio study of piezoelectricity and spontaneous polarization in ZnO. Phys Rev B, 1994, 50(15): 10715–10721
16 Molarius J, Kaitila J, Pensala T, et al. Piezoelectric ZnO films by r.f. sputtering. J Mater Sci-Mater El, 2003, 14(5-7): 431–435
17 Shibata T, Unno K, Makino E, et al. Characterization of sputtered ZnO thin film as sensor and actuator for diamond AFM probe. Sensor Actuat A-Phys, 2002, 102(1-2): 106–113
18 Zhao M H, Wang Z L, Mao S X. Piezoelectric characterization of individual zinc oxide nanobelt probed by piezoresponse force microscope. Nano Lett, 2004, 4(4): 587–590
19 Desai A V, Haque M A. Mechanical properties of ZnO nanowires. Sens Actuator A-Phys, 2007, 134(1): 169–176
20 Chen J J, Gao Y, Zeng F, et al. Effect of sputtering oxygen partial pressures on structure and physical properties of high resistivity ZnO films. Appl Surf Sci, 2004, 223(4): 318–329
21 Chen J J, Zeng F, Li D M, et al. Deposition of high-quality zinc oxide thin films on diamond substrates for high-frequency surface acoustic wave filter applications. Thin Solid Films, 2005, 485(1-2): 257–261
22 Chu S Y, Chen T Y, Water W. The investigation of preferred orientation growth of ZnO films on the $PbTiO_3$-based ceramics and its application for SAW devices. J Cryst Growth, 2003, 257(3-4): 280–285
23 Chen T Y, Chu S Y. The piezoelectric and dielectric properties of Ca-additive Sm-modified $PbTiO_3$ ceramics intended for surface acoustic wave devices. J Eur Ceram Soc, 2003, 23(12): 2171–2176
24 Chen T Y, Chu S Y, Cheng C K. Doping effects on the piezoelectric properties of low-temperature sintered $PbTiO_3$-based ceramics for SAW applications. Integr Ferroelectr, 2003, 58: 1315–1324
25 Chen T Y, Chu S Y, Juang Y D. Effects of strontium on the surface acoustic wave properties of Sm-modified $PbTiO_3$ ceramics. Ultrasonics, 2003, 41(2): 141–143
26 Chen T Y, Chu S Y, Wu S J, et al. Effects of strontium on the dielectric and piezoelectric properties of Sm-modified $PbTiO_3$ ceramics. Ferroelectrics, 2003, 282: 37–47
27 Chu S Y, Chen T Y. Strontium doping effects on the characteristics of Sm-modified $PbTiO_3$ ceramics. Sensor Actuat A-Phys, 2003, 107(1): 75–79
28 Ataev B M, Bagamadova A M, Djabrailov A M, et al. Highly conductive and transparent Ga-doped expitaxial ZnO films on sappire by CVD. Thin Solid Films, 1995, 260(1): 19–20
29 Myong S Y, Baik S J, Lee C H, et al. Extremely transparent and conductive ZnO:Al thin films prepared by photo-assisted metalorganic chemical vapor deposition (photo-MOCVD) using $AlCl_3(6H_{(2)}O)$ as new doping material. Jpn J Appl Phys, 1997, 36(8B): L1078–L1081
30 Pan F, Song C, Liu X J, et al. Ferromagnetism and possible application in spintronics of transition-metal-doped ZnO films. Mat Sci Eng R, 2008, 62(1): 1–35
31 Song C, Geng K W, Zeng F, et al. Giant magnetic moment in an anomalous ferromagnetic insulator: Co-doped ZnO. Phys Rev B, 2006, 73: 024405
32 Song C, Liu X J, Geng K W, et al. Transition from diluted magnetic insulator to semiconductor in Co-doped ZnO transparent oxide. J Appl Phys, 2007, 101: 103903
33 Song C, Pan S N, Liu X J, et al. Evidence of structural defect enhanced room-temperature ferromagnetism in Co-doped ZnO. J Phys-Condens Mat, 2007, 19: 176229
34 Song C, Zeng F, Geng K W, et al. Substrate-dependent magnetization in Co-doped ZnO insulating films. Phys Rev B, 2007, 76: 045215
35 Song C, Zeng F, Geng K W, et al. The magnetic properties of Co-doped ZnO diluted magnetic insulator films prepared by direct current reactive magnetron co-sputtering. J Magn Magn Mater, 2007, 309(1): 25–30
36 Luo J T, Zhu X Y, Fan B, et al. Microstructure and photoluminescence study of vanadium-doped ZnO films. J Phys D-Appl Phys, 2009, 42: 115109
37 Wang X B, Song C, Geng K W, et al. Photoluminescence and Raman scattering of Cu-doped ZnO films prepared by magnetron sputtering. Appl Surf Sci, 2007, 253(16): 6905–6909
38 Wang X B, Song C, Geng K W, et al. Luminescence and Raman scattering properties of Ag-doped ZnO films. J Phys D-Appl Phys, 2006, 39(23): 4992–4996
39 Pan F, Liu X J, Yang Y C, et al. Multiferroic and piezoelectric behavior of transition-metal doped ZnO films. Mater Sci Forum, 2009, 620-622: 735–740
40 Yang Y C, Song C, Wang X H, et al. Giant piezoelectric d_{33} coefficient in ferroelectric vanadium doped ZnO films. Appl Phys Lett, 2008, 92: 012907
41 Yang Y C, Song C, Wang X H, et al. Cr-substitution-induced ferroelectric and improved piezoelectric properties of $Zn_{1-x}Cr_xO$ films. J Appl Phys, 2008, 103: 074107
42 Luo J T, Yang Y C, Zhu X Y, et al. Enhanced electromechanical response of Fe-doped ZnO films by modulating the chemical state and ionic size of the Fe dopant. Phys Rev B, 2010, 82: 014116
43 Luo J T, Zhu X Y, Chen G, et al. Influence of the Mn concentration on the electromechanical response d_{33} of Mn-doped ZnO films. Phys Status Solidi-Rapid Res Lett, 2010, 4(8-9): 209–211
44 Xu X H, Blythe H J, Ziese M, et al. Carrier-induced ferromagnetism in n-type ZnMnAlO and ZnCoAlO thin films at room temperature. New J Phys, 2006, 8: 135
45 Xu Q, Hartmann L, Schmidt H, et al. s-d exchange interaction induced magnetoresistance in magnetic ZnO. Phys Rev B, 2007, 76: 134417
46 Bdikin I K, Gracio J, Ayouchi R, et al. Local piezoelectric properties of ZnO thin films prepared by RF-plasma-assisted pulsed-laser deposition method. Nanotechnology, 2010, 21: 235703
47 Lee J W, Subramaniam N G, Lee J C, et al. Study of stable p-type conductivity in bismuth-doped ZnO films grown by pulsed-laser deposition. Europhys Lett, 2011, 95: 47002
48 Prasad S V, Nainaparampil J J, Zabinski J S. Tribological behavior

of alumina doped zinc oxide films grown by pulsed laser deposition. J Vac Sci Technol A, 2002, 20(5): 1738–1743
49 Jeong S H, Park B N, Lee S B, et al. Study on the doping effect of Li-doped ZnO film. Thin Solid Films, 2008, 516(16): 5586–5589
50 Kawamura H, Yamada H, Takeuchi M, et al. Current-voltage characteristics of high-resistive ZnO thin films deposited by RF magnetron sputtering. Vacuum, 2004, 74(3-4): 567–570
51 Yang Y C, Song C, Zeng F, et al. V^{5+} ionic displacement induced ferroelectric behavior in V-doped ZnO films. Appl Phys Lett, 2007, 90: 242903
52 Ni H Q, Lu Y F, Liu Z Y, et al. Investigation of Li-doped ferroelectric and piezoelectric ZnO films by electric force microscopy and Raman spectroscopy. Appl Phys Lett, 2001, 79(6): 812–814
53 Nicolescu M, Anastasescu M, Preda S, et al. Investigation of microstructural properties of nitrogen doped ZnO thin films formed by magnetron sputtering on silicon substrate. J Optoelectron Adv M, 2010, 12(5): 1045–1051
54 Shao W D, Chen X F, Ren W, et al. V-doped ZnO thin films prepared by RF magnetron sputtering C-8551-2011. Ferroelectrics, 2010, 406: 10–15
55 Water W, Chu S Y, Juang Y D, et al. Li_2CO_3-doped ZnO films prepared by RF magnetron sputtering technique for acoustic device application. Mater Lett, 2002, 57(4): 998–1003
56 Liu H Y, Avrutin V, Izyumskaya N, et al. Highly conductive and optically transparent GZO films grown under metal-rich conditions by plasma assisted MBE. Phys Status Solidi-Rapid Res Lett, 2010, 4(3-4): 70–72
57 Seghier D, Gislason H P. Effects of cobalt doping on the electrical properties of MBE-grown ZnO. J Mater Sci-Mater El, 2011, 22(9): 1400–1403
58 Sun J W, Lu Y M, Liu Y C, et al. The activation energy of the nitrogen acceptor in p-type ZnO film grown by plasma-assisted molecular beam epitaxy. Solid State Commun, 2006, 140(7-8): 345–348
59 Wang X, Lu Y M, Shen D Z, et al. Electrical properties of N-doped ZnO grown on sapphire by P-MBE. Semicond Sci Tech, 2007, 22(2): 65–69
60 Zhang X A, Zhang J W, Zhang W F, et al. Enhancement-mode thin film transistor with nitrogen-doped ZnO channel layer deposited by laser molecular beam epitaxy. Thin Solid Films, 2008, 516(10): 3305–3308
61 Han S K, Lee H S, Lim D S, et al. Effects of gallium doping on properties of a-plane ZnO films on r-plane sapphire substrates by plasma-assisted molecular beam epitaxy. J Vac Sci Technol A, 2011, 29(3): 03A111
62 Zhang W Y, He D K, Liu Z Z, et al. Preparation of transparent conducting Al-doped ZnO thin films by single source chemical vapor deposition. Optoelectron Adv Mater-Rapid Commun, 2010, 4(11): 1651–1654
63 Chongsri K, Boonruang S, Techitdheera W, et al. N-doped MgZnO alloy thin film prepared by sol-gel method. Mater Lett, 2011, 65(12): 1842–1845
64 Kandjani A E, Tabriz M F, Moradi O M, et al. An investigation on linear optical properties of dilute Cr doped ZnO thin films synthesized via sol-gel process. J Alloy Compd, 2011, 509(30): 7854–7860
65 Ravichandran C, Srinivasan G, Lennon C, et al. Influence of post-deposition annealing on the structural, optical and electrical properties of Li and Mg co-doped ZnO thin films deposited by sol-gel technique. Superlattice Microst, 2011, 49(5): 527–536
66 Singh A, Kumar D, Khanna P K, et al. Anomalous behavior in ZnMgO thin films deposited by sol-gel method. Thin Solid Films, 2011, 519(17SI): 5826–5830
67 Tsay C Y, Wu C W, Lei C M, et al. Microstructural and optical properties of Ga-doped ZnO semiconductor thin films prepared by sol-gel process. Thin Solid Films, 2010, 519(5SI): 1516–1520
68 Ferblantier G, Mailly F, Al Asmar R, et al. Deposition of zinc oxide thin films for application in bulk acoustic wave resonator. Sensor Actuat A-Phys, 2005, 122(2): 184–188
69 Lee J B, Kim H J, Kim S G, et al. Deposition of ZnO thin films by magnetron sputtering for a film bulk acoustic resonator. Thin Solid Films, 2003, (1-2): 179–185
70 Emanetoglua N W, Gorlab C, Liua Y, et al. Epitaxial ZnO piezoelectric thin films for saw filters. Mater Sci Semicond Process, 1999, 2(3): 247–252
71 Nakahata H, Fujii S, Higaki K, et al. Diamond-based surface acoustic wave devices. Semicond Sci Tech, 2003, 18S(3): S96–S104
72 Yoshino Y. Piezoelectric thin films and their applications for electronics. J Appl Phys, 2009, 105: 061623
73 Ozgur U, Alivov Y I, Liu C, et al. A comprehensive review of ZnO materials and devices. J Appl Phys, 2005, 98: 041301
74 Chen L X, Li C M, Yin W L, et al. Effect of deposition temperature and quality of free-standing diamond substrates on the properties of RF sputtering ZnO films. Diam Relat Mater, 2011, 20(4): 527–531
75 Chiang Y C Y, Sung C C, Ro R. Effects of metal buffer layer on characteristics of surface acoustic waves in ZnO/metal/diamond structures. Appl Phys Lett, 2010, 96: 154104
76 Phan D T, Suh H C, Chung G S. Surface acoustic wave characteristics of ZnO films grown on a polycrystalline 3C-SiC buffer layer. Microelectron Eng, 2011, 88(1): 105–108
77 Shih W C, Huang R C. Fabrication of high frequency ZnO thin film SAW devices on silicon substrate with a diamond-like carbon buffer layer using RF magnetron sputtering. Vacuum, 2008, 83(3): 675–678
78 Le Brizoual L, Sarry F, Elmazria O, et al. GHz frequency ZnO/Si SAW device. IEEE T Ultrason Ferr, 2008, 55(2): 442–450
79 Wei C L, Chen Y C, Cheng C C, et al. Highly sensitive ultraviolet detector using a ZnO/Si layered SAW oscillator. Thin Solid Films, 2010, 518(11): 3059–3062
80 Jung J P, Lee J B, Kim J S, et al. Fabrication and characterization of high frequency SAW device with IDT/ZnO/AlN/Si configuration: Role of AlN buffer. Thin Solid Films, 2004, 447: 605–609
81 Kim H. Surface acoustic wave properties in ZnO/AlN/Si structure. J Korean Phys Soc, 1998, 32(4): S1741–S1743
82 Krishnamoorthy S, Iliadis A A. Properties of high sensitivity ZnO surface acoustic wave sensors on SiO_2/(100) Si substrates. Solid State Electron, 2008, 52(11): 1710–1716
83 Krishnamoorthy S, Iliadis A A. Development of high frequency ZnO/SiO_2/Si Love mode surface acoustic wave devices. Solid State Electron, 2006, 50(6): 1113–1118
84 Krishnamoorthy S, Iliadis A A, Bei T, et al. An interleukin-6 ZnO/SiO_2/Si surface acoustic wave biosensor. Biosens Bioelectron, 2008, 24(2): 313–318
85 Chang R C, Chu S Y, Yeh P W, et al. An investigation of Love wave devices based on ZnO: Mg/$LiNbO_3$ structure. Sensor Actuat B-Chem, 2008, 132(1): 312–318
86 Coey J, Douvalis A P, Fitzgerald C B, et al. Ferromagnetism in Fe-doped SnO_2 thin films. Appl Phys Lett, 2004, 84(8): 1332–1334
87 Ramachandran S, Tiwari A, Narayan J. $Zn_{0.9}Co_{0.1}O$-based diluted magnetic semiconducting thin films. Appl Phys Lett, 2004, 84(25): 5255–5257
88 Ueda K, Tabata H, Kawai T. Magnetic and electric properties of transition-metal-doped ZnO films. Appl Phys Lett, 2001, 79(7): 988–990
89 Chiou J W, Chang S Y, Huang W H, et al. The characterization of Cr secondary oxide phases in ZnO films studied by X-ray spectroscopy and photoemission spectroscopy. Appl Surf Sci, 2011, 257(11): 4863–4866
90 Reddy K M, Benson R, Hays J, et al. On the room-temperature ferromagnetism of $Zn_{1-x}Cr_xO$ thin films deposited by reactive co-sputtering. Sol Energ Mat Sol C, 2007, 91(15-16): 1496–1502
91 Song Y Y, Quang P H, Lim K S, et al. Ferromagnetism above room temperature in Cr-doped AlN films. J Korean Phys Soc, 2006, 48(6): 1449–1453
92 Wang B Q, Iqbal J, Shan X D, et al. Effects of Cr-doping on the

photoluminescence and ferromagnetism at room temperature in ZnO nanomaterials prepared by soft chemistry route. Mater Chem Phys, 2009, 113(1): 103–106
93 Bordage A, Brouder C, Balan E, et al. Electronic structure and local environment of substitutional V^{3+} in grossular garnet $Ca_3Al(SiO_4)_3$: K-edge X-ray absorption spectroscopy and first-principles modeling. Am Mineral, 2010, 95(8-9): 1161–1171
94 Engemann C, Hormes J, Longen A, et al. An X-ray absorption near edge spectroscopy (XANES) study on organochromium complexes at the Cr *K*-edge. Chem Phys, 1998, 237(3): 471–481
95 Frommer J, Nachtegaal M, Czekaj I, et al. The Cr X-ray absorption K-edge structure of poorly crystalline Fe(III)-Cr(III)-oxyhydroxides. Am Mineral, 2010, 95(8-9): 1202–1213
96 Goering E, Bayer A, Gold S, et al. Direct correlation of Cr 3d orbital polarization and O K-edge X-ray magnetic circular dichroism of epitaxial CrO_2 films. Europhys Lett, 2002, 58(6): 906–911
97 Miyano K E, Woicik J C, Devi P S, et al. Cr K edge x-ray absorption study of Cr dopants in Mg_2SiO_4 and Ca_2GeO_4. Appl Phys Lett, 1997, 71(9): 1168–1170
98 Ahlers S, Stone P R, Sircar N, et al. Comparison of the magnetic properties of GeMn thin films through Mn *L*-edge x-ray absorption. Appl Phys Lett, 2009, 95: 151911
99 Farrell S P, Fleet M E, Stekhin I E, et al. Evolution of local electronic structure in alabandite and niningerite solid solutions [(Mn,Fe)S, (Mg, Mn)S, (Mg,Fe)S] using sulfur *K*- and *L*-edge XANES spectroscopy. Am Mineral, 2002, 87(10): 1321–1332
100 Hocking R K, George S D, Gross Z, et al. Fe *L*- and *K*-edge XAS of low-spin ferric corrole: Bonding and reactivity relative to low-spin ferric porphyrin. Inorg Chem, 2009, 48(4): 1678–1688
101 Ikeno H, Tanaka I, Miyamae L, et al. First principles calculation of Fe L_2,L_3-edge X-ray absorption near edge structures of iron oxides. Mater Trans, 2004, 45(5): 1414–1418
102 Meneses C T, Vicentin F C, Sasaki J M, et al. Influence of Li on the K-edge of O and L_2,L_3 of the Mn XANES in $Li_xMn_2O_4$ thin films. J Electron Spectrosc, 2007, 156: 326–328
103 Saini N L, Wakisaka Y, Joseph B, et al. Electronic structure of $FeSe_{1-x}Te_x$ studied by Fe $L_{(2,3)}$-edge x-ray absorption spectroscopy. Phys Rev B, 2011, 83: 052502
104 Stojic N, Binggeli N, Altarelli M. Mn L_2,L_3 edge resonant x-ray scattering in manganites: Influence of the magnetic state. Phys Rev B, 2005, 72: 104108
105 Taguchi M, Altarellli M. Orbital ordering in $LaMnO_3$: Cluster model calculation of resonant X-ray scattering and X-ray absorption at the Mn L_2,L_3 edge. Surf Rev Lett, 2002, 9(2): 1167–1171
106 Christman J A, Woolcott R R, Kingon A I, et al. Piezoelectric measurements with atomic force microscopy. Appl Phys Lett, 1998, 73(26): 3851–3853
107 Dubois M A, Muralt P. Measurement of the effective transverse piezoelectric coefficient $e_{(31,f)}$ of AlN and $Pb(Zr_xTi_{1-x})O_3$ thin films. Sensor Actuat A-Phys, 1999, 77(2): 106–112
108 Kuffer O, Maggio-Aprile I, Triscone J M, et al. Piezoelectric response of epitaxial $Pb(Zr_{0.2}Ti_{0.8})O_3$ films measured by scanning tunneling microscopy. Appl Phys Lett, 2000, 77(11): 1701–1703
109 Yao K, Tay F. Measurement of longitudinal piezoelectric coefficient of thin films by a laser-scanning vibrometer. IEEE T Ultrason Ferr, 2003, 50(2): 113–116
110 Kalinin S V, Bonnell D A. Imaging mechanism of piezoresponse force microscopy of ferroelectric surfaces. Phys Rev B, 2002, 65: 125408
111 Zou C W, Li M, Wang H J, et al. Ferroelectricity in Li-implanted ZnO thin films. Nucl Instrum Methods Phys Res Sect B-Beam Interact Mater Atoms, 2009, 267(7): 1067–1071
112 Hotta Y, Rokuta E, Tabata H, et al. Optimization of electronic-band alignments at ferroelectric $(Zn_xCd_{1-x})S$/Si(100) interfaces. Appl Phys Lett, 2001, 78(21): 3283–3285
113 Islam Q T, Bunker B A. Ferroelectric transition in $Pb_{1-x}Ge_xTe$-extended X-ray absorption fine-structure investigation of the Ge and Pb sites. Phys Rev Lett, 1987, 59(23): 2701–2704
114 Onodera A, Tamaki N, Jin K, et al. Ferroelectric properties in piezoelectric semiconductor $Zn_{1-x}M_xO$ (M=Li, Mg). Jpn J Appl Phys, 1997, 36(9B): 6008–6011
115 Weil R, Nkum R, Muranevich E, et al. Ferroelectricity in Zinc-Cadmium telluride. Phys Rev Lett, 1989, 62(23): 2744–2746
116 Shulman R G, Yafet Y, Eisenberger P, et al. Observation and interpertation of X-ray absorption edges in Fe compounds and proteins. P Natl Acad Sci USA, 1976, 73(5): 1384–1388
117 Bair R A, Goddard W A. AB-initio studies of X-ray absorption-edge in copper-complexes. Phys Rev B, 1980, 22(6): 2767–2776
118 Wong J, Lytle F W, Messmer R P, et al. *K*-edge absorption-spectra of selected vanadium compounds. Phys Rev B, 1984, 30(10): 5596–5610
119 Purans J, Balzarotti A, Motta N, et al. EXAFS and XANES studies of local order in oxide glasses-manganese impurity defects and vanadium low-symmertry complexes. J Non-Cryst Solids, 1987, 94(3): 336–344
120 Kholkin A L, Akdogan E K, Safari A, et al. Characterization of the effective electrostriction coefficients in ferroelectric thin films. J Appl Phys, 2001, 89(12): 8066–8073
121 Dhananjay, Nagaraju J, Krupanidhi S B. Effect of Li substitution on dielectric and ferroelectric properties of ZnO thin films grown by pulsed-laser ablation. J Appl Phys, 2006, 99: 0341053
122 Karanth D, Fu H X. Large electromechanical response in ZnO and its microscopic origin. Phys Rev B, 2005, 72: 064116
123 Chen Y Q, Zheng X J, Feng X. The fabrication of vanadium-doped ZnO piezoelectric nanofiber by electrospinning. Nanotechnology, 2010, 21: 055708
124 Maetaki A, Yamamoto M, Matsumoto H, et al. The preparation of ultra-thin chromium-vanadium oxides on Cu(100) studied by XPS and LEED. Surf Sci, 2000, 445(1): 80–88
125 Luo J T, Fan B, Zeng F, et al. Influence of Cr-doping on microstructure and piezoelectric response of AlN films. J Phys-D Appl Phys, 2009, 42: 2354069
126 Ankudinov A L, Ravel B, Rehr J J, et al. Real-space multiple-scattering calculation and interpretation of x-ray-absorption near-edge structure. Phys Rev B, 1998, 58(12): 7565–7576
127 Garg K B, Saini N L, Sekhar B R, et al. Doped holes and Mn valence in manganites: A polarized soft x-ray absorption study of $LaMnO_3$ and quasi-2D manganite systems. J Phys-Condens Mat, 2008, 20: 055215
128 Bondino F, Garg K B, Magnano E, et al. Electronic structure of Mn-doped ZnO by x-ray emission and absorption spectroscopy. J Phys-Condens Mat, 2008, 20: 275205
129 Thakur P, Chae K H, Kim J Y, et al. X-ray absorption and magnetic circular dichroism characterizations of Mn doped ZnO. Appl Phys Lett, 2007, 91: 162503
130 Kumar S, Kim Y J, Koo B H, et al. Structural and magnetic properties of chemically synthesized Fe doped ZnO. J Appl Phys, 2009, 105(7): 07C520
131 Wang L M, Liao J W, Peng Z A, et al. Doping effects on the characteristics of Fe:ZnO films: Valence transition and hopping transport. J Electrochem Soc, 2009, 156(2): H138–H142
132 Wu P, Saraf G, Lu Y, et al. Ferromagnetism in Fe-implanted a-plane ZnO films. Appl Phys Lett, 2006, 89: 012508
133 Kang J S, Lee H J, Kim G, et al. Electronic structure of the cubic perovskite $SrMn_{1-x}Fe_xO_3$ investigated by x-ray spectroscopies. Phys Rev B, 2008, 78: 054434
134 Regan T J, Ohldag H, Stamm C, et al. Chemical effects at metal/oxide interfaces studied by x-ray-absorption spectroscopy. Phys Rev B, 2001, 64(21): 214422
135 Choi B J, Choi S, Eom T, et al. Influence of substrates on the nucleation and growth behaviors of $Ge_2Sb_2Te_5$ Films by combined plasma-enhanced atomic layer and Chemical Vapor Deposition. Chem Mater, 2009, 21(12): 2386–2396
136 Yamashita T, Hayes P. Analysis of XPS spectra of Fe^{2+} and Fe^{3+} ions in oxide materials. Appl Surf Sci, 2008, 254(8): 2441–2449
137 Gupta A, Kumar A, Waghmare U V, et al. Origin of activation of

lattice oxygen and synergistic interaction in bimetal-ionic $Ce_{0.89}Fe_{0.1}Pd_{0.01}O$(2-delta) catalyst. Chem Mater, 2009, 21(20): 4880–4891

138 Mills P, Sullivan J L. A study of the core level electrons in Fe and its 3 oxides by means of X-ray photoelectron-spectroscopy. J Phys D-Appl Phys, 1983, 16(5): 723–732

139 Assouar M B, Elmazria O, Rioboo R J, et al. Modelling of SAW filter based on ZnO/diamond/Si layered structure including velocity dispersion. Appl Surf Sci, 2000, 164: 200–204

140 Zhu J, Chen Y, Saraf G, et al. Voltage tunable surface acoustic wave phase shifter using semiconducting/piezoelectric ZnO dual layers grown on r-Al_2O_3. Appl Phys Lett, 2006, 89: 103513

141 Hachigo A, Nakahata H, Higaki K, et al. Heteroepitaxial growth of ZnO films on diamond (111) plane by magnetron sputtering. Appl Phys Lett, 1994, 65(20): 2556–2558

142 Makkonen T, Plessky V P, Steichen W, et al. Surface-acoustic-wave devices for the 2.5–5 GHz frequency range based on longitudinal leaky waves. Appl Phys Lett, 2003, 82(19): 3351–3353

143 Luo J T, Zeng F, Pan F, et al. Filtering performance improvement in V-doped ZnO/diamond surface acoustic wave filters. Appl Surf Sci, 2010, 256(10): 3081–3085

144 Emanetoglu N W, Muthukumar S, Wittstruck R H, et al. $Mg_xZn_{1-x}O$: A new piezoelectric material. IEEE T Ultrason Ferr, 2003, 50(5): 537–543

145 Wittstruck R H, Tong X J, Emanetoglu N W, et al. Characteristics of $Mg_xZn_{1-x}O$ thin film bulk acoustic wave devices. IEEE T Ultrason Ferr, 2003, 50(10): 1272–1278

146 Chen Y, Saraf G, Lu Y C, et al. a-plane $Mg_xZn_{1-x}O$ films deposited on r-sapphire and its surface acoustic wave characteristics. J Vac Sci Technol A, 2007, 25(4): 857–861

147 Water W, Yan Y S, Meen T H. Effect of magnesium doping on the structural and piezoelectric properties of sputtered ZnO thin film. Sensor Actuat A-Phys, 2008, 144(1): 105–108

148 Chang R C, Chu S Y, Yeh P W, et al. The influence of Mg doped ZnO thin films on the properties of love wave sensors. Sensor Actuat B-Chem, 2008, 132(1): 290–295

149 Ieki H, Kadota M. ZnO thin films for high frequency SAW devices. IEEE Ultrasonics Syposium, 1999: 281–289

150 Lee J B, Lee H J, Seo S H, et al. Characterization of undoped and Cu-doped ZnO films for surface acoustic wave applications. Thin Solid Films, 2001, 398: 641–646

151 Water W, Yang Y S. The influence of calcium doped ZnO films on love wave sensor characteristics. Sensor Actuat A-Phys, 2006, 127(2): 360–365